The 2dF Galaxy Redshift Survey: the power spectrum and the matter content of the Universe

Will J. Percival,[1][★] Carlton M. Baugh,[2] Joss Bland-Hawthorn,[3] Terry Bridges,[3] Russell Cannon,[3] Shaun Cole,[2] Matthew Colless,[4] Chris Collins,[5] Warrick Couch,[6] Gavin Dalton,[7] Roberto De Propris,[6] Simon P. Driver,[8] George Efstathiou,[9] Richard S. Ellis,[10] Carlos S. Frenk,[2] Karl Glazebrook,[11] Carole Jackson,[4] Ofer Lahav,[9] Ian Lewis,[3] Stuart Lumsden,[12] Steve Maddox,[13] Stephen Moody,[9] Peder Norberg,[2] John A. Peacock,[1] Bruce A. Peterson,[4] Will Sutherland[1] and Keith Taylor[3]

[1]*Institute for Astronomy, University of Edinburgh, Royal Observatory, Blackford Hill, Edinburgh EH9 3HJ*
[2]*Department of Physics, University of Durham, South Road, Durham DH1 3LE*
[3]*Anglo-Australian Observatory, P. O. Box 296, Epping, NSW 2121, Australia*
[4]*Research School of Astronomy & Astrophysics, The Australian National University, Weston Creek, ACT 2611, Australia*
[5]*Astrophysics Research Institute, Liverpool John Moores University, Twelve Quays House, Birkenhead, L14 1LD*
[6]*Department of Astrophysics, University of New South Wales, Sydney, NSW 2052, Australia*
[7]*Department of Physics, University of Oxford, Keble Road, Oxford OX1 3RH*
[8]*School of Physics and Astronomy, University of St Andrews, North Haugh, St Andrews, Fife, KY6 9SS*
[9]*Institute of Astronomy, University of Cambridge, Madingley Road, Cambridge CB3 0HA*
[10]*Department of Astronomy, Caltech, Pasadena, CA 91125, USA*
[11]*Department of Physics & Astronomy, Johns Hopkins University, Baltimore, MD 21218-2686, USA*
[12]*Department of Physics, University of Leeds, Woodhouse Lane, Leeds, LS2 9JT*
[13]*School of Physics & Astronomy, University of Nottingham, Nottingham NG7 2RD*

ABSTRACT

The 2dF Galaxy Redshift Survey has now measured in excess of 160 000 galaxy redshifts. This paper presents the power spectrum of the galaxy distribution, calculated using a direct Fourier transform based technique. We argue that, within the k-space region $0.02 \lesssim k \lesssim 0.15\,h\,\mathrm{Mpc}^{-1}$, the shape of this spectrum should be close to that of the linear density perturbations convolved with the window function of the survey. This window function and its convolving effect on the power spectrum estimate are analysed in detail. By convolving model spectra, we are able to fit the power-spectrum data and provide a measure of the matter content of the Universe. Our results show that models containing baryon oscillations are mildly preferred over featureless power spectra. Analysis of the data yields 68 per cent confidence limits on the total matter density times the Hubble parameter $\Omega_{\mathrm{m}} h = 0.20 \pm 0.03$, and the baryon fraction $\Omega_{\mathrm{b}}/\Omega_{\mathrm{m}} = 0.15 \pm 0.07$, assuming scale-invariant primordial fluctuations.

Key words: cosmological parameters – large-scale structure of Universe.

1 INTRODUCTION

Present-day cosmological structure is thought to have formed by the gravitational amplification of small density perturbations. These fluctuations are readily quantified in terms of their Fourier modes via the power spectrum, which is a statistically complete description for a Gaussian field. The power spectrum is also of direct physical interest, because it encodes information about the formation of the primordial fluctuations, and especially about how these are modified according to the matter content of the Universe.

In this paper, we present an estimate of the power spectrum of the galaxy distribution in the 2dF Galaxy Redshift Survey (2dFGRS). The 2dFGRS is designed around the 2dF multi-fibre spectrograph on the Anglo-Australian Telescope, which is capable of obtaining spectra for up to 400 objects simultaneously over a 2° diameter field of view. Full details of the instrument and its

★E-mail: wjp@roe.ac.uk

performance are given in Lewis et al. (2000). See also http://www. aao.gov.au/2df/. The survey aims to obtain redshifts for 250 000 galaxies to an extinction-corrected magnitude limit of $b_J < 19.45$. A description of the survey is given by Colless et al. (2001); full details of the present status can be obtained from http://www.mso. anu.edu.au/2dFGRS/.

At the time of writing, the 2dFGRS is the largest existing galaxy redshift survey, following a natural progression from studies such as the CfA survey (Huchra et al. 1990), the LCRS (Shectman et al. 1996), and the PSCz survey (Saunders et al. 2000). The data and analysis presented in this paper covers the sample with 166 490 redshifts observed prior to 2001 February. A sample of this size allows large-scale structure statistics to be measured with very small random errors, and we present an initial power-spectrum analysis of the 2dFGRS here. Section 2 details some of the practical issues concerning sample selection, and Section 3 discusses power-spectrum estimation. The survey coverage in angular position and redshift is relatively complex, and the convolving effects of the survey window are significant compared to the small random errors. These effects are therefore studied in some detail, both analytically and in comparison to mock data, in Section 4. This leads to a robust estimate of the covariance matrix for the estimates of the power at different wavenumbers, which is presented in Section 5. The covariance matrix allows proper likelihood-based model fitting, which is carried out in Section 6. The power-spectrum fits clearly indicate a low-density universe with $\Omega_m h \simeq 0.2$, in agreement with many past studies. We also show that the preferred model requires a degree of baryon oscillations in the power spectrum, corresponding to a baryonic fraction of about 15 per cent. We conclude by considering the consistency between this picture and other lines of evidence.

2 THE 2DFGRS SAMPLE

2.1 The angular mask

When complete, the angular geometry of the 2dFGRS will consist of two declination strips plus 100 random $2°$ fields. One strip is near the Southern Galactic Pole (SGP) and covers approximately $85° \times 15°$; the other strip is near the Northern Galactic Pole (NGP) and covers $75° \times 10°$. These strips are not coplanar, which is a significant factor in using the survey to measure 3D structure. The 100 random fields are spread uniformly over a 7000 deg^2 region near the SGP; the present analysis includes 71 of these fields.

The input catalogue is a revised and extended version of the APM galaxy catalogue (Maddox et al. 1990a,b; Maddox, Efstathiou & Sutherland 1990c, 1996). This includes over 5×10^6 galaxies down to $b_J = 20.5$ over $\sim 10^4$ deg^2. The APM catalogue was used previously to recover the 3D power spectrum of galaxies by inverting the appropriate integral equations (Baugh & Efstathiou 1993; Efstathiou & Moody 2001). However, these techniques are demanding in sample variance and photometric uniformity, and we expect that a fully 3D analysis should yield a more robust result.

An adaptive tiling algorithm is employed to cover the survey area with a minimum number of overlapping 2dF fields. With this algorithm we are able to achieve a 93 per cent sampling rate with on average fewer than 5 per cent wasted fibres per field. Over the whole area of the survey there are in excess of 250 000 galaxies. At the present intermediate stage of the survey, unobserved fields mean that the proportion of targets with known redshifts is a strongly varying function of position. In addition, regions around bright stars are omitted, so the 2dFGRS angular mask is a complicated pattern on the sky (see e.g. Colless et al. 2001). Nevertheless, because the tiling algorithm is known, it is possible to generate random catalogues that are subject to the same selection effects. A number of different codes have been written to achieve this task, with consistent results. Furthermore, because a 3D power spectrum analysis averages over directions, small imperfections in reproducing the sky pattern of the real data tend to wash out. For example, we tried adding magnitude offset errors of $\Delta M = \pm 0.2$ in each $5°$ Schmidt field, but the power spectrum did not change significantly.

Given the sampling pattern on the sky, there are two possible analysis strategies: one can either build a similar variation into any random catalogue, or the analysis can use a uniform random catalogue, weighting each galaxy by the reciprocal of the sampling. The former strategy is superior in terms of shot noise, but the latter is necessary if the mask is correlated with real structure (e.g. fibre crowding problems in high-density regions). We obtain almost identical results with either strategy, demonstrating that the adaptive tiling has achieved its target of uniform selection of targets.

2.2 Redshift selection

The sample is chosen to be magnitude-limited at $b_J = 19.45$ after extinction-correcting all the magnitudes in the APM catalogue (Schlegel, Finkbeiner & Davis 1998). This limit was chosen because the mean number of galaxies per square degree then matches the density of fibres available with 2dF. The resulting distribution of galaxy redshifts $n(z)\,dz$ has a median of approximately 0.11, and can be fitted by

$$n(z)\,dz \propto \frac{(z/z_c)^{\gamma-1}}{[1 + (z/z_c)^{\gamma/\beta}]^{1+\beta}}\,dz, \tag{1}$$

where z_c, γ and β are fitted parameters. Fitting to all of the galaxy redshifts gives $z_c = 0.144$, $\gamma = 2.21$ and $\beta = 0.554$. However, the redshift distribution is expected to vary with position on the sky, because the survey depth is not completely uniform. This arises because the spectroscopic success rate is a function of apparent magnitude: data from poorer nights are biased to brighter objects, and thus to lower redshifts. Also, our estimates of galactic extinction and CCD calibration of the zero points of the individual photographic plates have been revised since the original input catalogue was defined. All these effects contribute to a modulation of the depth of the survey, which is accounted for when making the random catalogue that defines the survey volume. Because these estimates of non-uniformity can never be very precise, we have chosen to allow the parameters of the $n(z)$ fit to be different in distinct zones of the sky, treating the NGP, SGP and random fields separately. Analysis of mock catalogues shows that this makes only a small difference to the power estimates at $k > 0.02\,h\,\mathrm{Mpc}^{-1}$, which we use as our normal analysis limit.

3 ESTIMATING THE POWER SPECTRUM

3.1 The FKP method

Following the Fourier transform based approach of Feldman, Kaiser & Peacock (1994, hereafter FKP), each galaxy in the sample was placed onto a $512 \times 512 \times 256$ grid, scaled to cover the

entire sample in each direction. The size of the cuboid that just contains all of the data to a redshift limit at $z = 0.25$ is $1388 \times 1017 \times 685\,h^{-3}\,\mathrm{Mpc}^3$, assuming a flat $\Omega_m = 0.3$ cosmology. The grid used therefore leads to approximately equal Nyquist frequencies in each direction. For this grid, $k = 0.15\,h\,\mathrm{Mpc}^{-1}$ corresponds to a conservative 13 per cent of the minimum Nyquist frequency. Comparing this with results obtained using different size grids also suggests that aliasing is not a problem for frequencies $k < 0.15\,h\,\mathrm{Mpc}^{-1}$, although, of course, it will affect the result at large k. As shown by FKP, the galaxies must be weighted in order to optimize the balance between cosmic variance and shot noise. Assuming that the fluctuations are Gaussian, the optimal FKP weight is

$$w(z, \theta, \phi) = \frac{1}{[1 + \bar{P}\bar{n}(z, \theta, \phi)]}, \tag{2}$$

where $\bar{n}(z, \theta, \phi)$ is the expected galaxy density. A value of $\bar{P} = 5000\,h^{-3}\,\mathrm{Mpc}^3$ was assumed, but this is not critical. For a high-density sample like the 2dFGRS, one very nearly gives equal weight to each volume element, independent of $\bar{P}$. We applied an upper redshift limit of $z = 0.25$, to remove regions with a very low galaxy density where the choice of $\bar{P}$ would matter. We also defined a lower limit of $z > 0.003$. With restriction to objects with redshift quality flag ≥ 3, this leaves a sample of 147 024 objects.

In order to transform from redshifts to distances in $h\,\mathrm{Mpc}$, we need to assume values for Ω_m and Ω_v. Strictly, when fitting models to the data we should alter these values to match the model. However, the power spectrum is only weakly dependent on this choice: we have tried both an Einstein–de Sitter cosmology and a flat $\Omega_m = 0.3$ cosmology and find approximately the same best-fitting model parameters (see Table 1). Normally, we will present results for a flat $\Omega_m = 0.3$ cosmology.

Before Fourier transforming the data, we need to convert from a distribution of galaxies to a distribution of overdensities. To do this, the survey volume was defined by a random catalogue that mimics the sampling of the original data. In order to create such a sample, we have used the known angular position and completeness of each field (described in Section 2.1), coupled with an empirically determined fit to the redshift distribution of the 2dFGRS catalogue (described in Section 2.2). The variations in observing conditions, and the corresponding spectroscopic success rate, mean that there are in practice variations in the survey depth with sky position. These are allowed for by appropriate perturbations of the redshift distribution in the random catalogue, although this again turns out to be an unimportant effect. The random catalogue we created had five times the number of points in the galaxy catalogue.

Having Fourier transformed the resulting overdensity field, we simply subtracted the shot noise contribution from the result, and re-normalized $P(k)$ in order to correct for a differing sample volume and Fourier transform volume, and to correct for the weighting (FKP equations 2.1.3 and 2.1.10). $P(k)$ was then spherically averaged over k-space shells.

The power spectrum of the galaxy distribution needs to be interpreted with care, as it is altered from that of the initial density fluctuations (the linear power spectrum) by a number of effects:

(i) The collapse of structures. The mass no longer obeys the linear power spectrum on small scales after it has undergone non-linear collapse.

(ii) Galaxies are not expected to form a Poisson sampling of the underlying mass fluctuations, and are biased with respect to this distribution.

(iii) Random oscillations of galaxies within larger collapsed objects causes 'Fingers of God' redshift space distortions that damp the estimates of the small-scale power.

(iv) The infall of galaxies into concentrations of mass on large scales (Kaiser 1987) enhances the observed power in the radial direction, creating a large-scale redshift distortion.

Additionally, the recovered power spectrum estimated using the FKP approach is the convolution of the galaxy power spectrum with the 'window function' $|W_k|^2$ of the survey [W_k being the Fourier transform of the product of the survey mask and redshift selection function times $w(z)$; see FKP equation 2.1.7]:

$$\hat{P}_{\mathrm{FKP}}(\mathbf{k}) \propto \int P_{\mathrm{true}}(\mathbf{k} - \mathbf{q})|W_k(\mathbf{q})|^2\,\mathrm{d}^3\mathbf{q}. \tag{3}$$

In Section 3.2 we show how we may model the effect of the window function, by convolving power spectra with an analytic fit to the spherically averaged window function, and empirically by analysing realizations of Gaussian density fields within the survey region. The inverse problem of deconvolving the window function from the power spectrum is not attempted in this work.

3.2 The window function

The 2dFGRS window function $|W_k|^2$ is not compact, and has a significant effect on the recovered power spectrum. Although W_k is anisotropic as a result of the complicated real-space selection function, we are normally interested in the spherical average of the final power spectrum over k-space shells. Therefore, if P_{true} is isotropic, we obtain the same result by convolving just with the spherical average of $|W_k|^2$. A good approximation to the averaged window is

$$\langle|W_k|^2\rangle = [1 + (k/0.00342)^2 + (k/0.00983)^4]^{-1}. \tag{4}$$

This fit is compared to the exact 2dFGRS window in Fig. 1. The potential cause of problems is the tail to high k. The convolution involves a normalization factor $\int|W_k|^2 4\pi k^2\,\mathrm{d}k$, and a significant part of this volume lies outside the 'core', which has a scale of $0.003\,h\,\mathrm{Mpc}^{-1}$. In this respect, the 2dFGRS window is quite like an adaptive-optics point-spread function.

Of course, redshift-space distortions mean that the true power spectrum will not be strictly isotropic in practice. However, the simulation results described below suggest that the effect of such deviations are small and do not have a significant impact on the recovered power spectrum.

In order to demonstrate the effect of this window function on power spectra, we have sampled realizations of a linear density field covering the volume of the 2dFGRS data. Averaging the results of this analysis for 1000 realizations with different phases, and comparing with the true input power spectrum, we can quantify the effect of the window function. This is shown in Fig. 2 for spectra corresponding to two different cosmologies. The shape of the spectra are significantly altered, and any oscillations are damped. Analytically convolving the power spectra with the fit to the window function given by equation (4) provides the same result.

Because the random catalogue is scaled to match the normalization of the galaxy catalogue, the average overdensity is artificially set to zero, forcing $P(0) = 0$. This self-normalization results in a deficit in the measured power spectrum, equivalent to subtracting a scaled copy of the window function centred on $k = 0$. However, this is a very small effect in the regime of interest

because $|W_k|^2$ is a rapidly decreasing function of k (see Fig. 1), and $P(k)$ is expected to be an increasing function of k for small k. The effect of this self-normalization is shown in Fig. 2 for model power spectra.

3.3 Results

The recovered 2dFGRS power spectrum is presented in Fig. 3. To highlight features in the spectra presented in this paper, we have plotted their ratio with a smooth cold dark matter (CDM) power spectrum $P(k, \Omega_m h = 0.2, \Omega_b/\Omega_m = 0)$ that has no baryon features. We also take a normalization of $\sigma_8 = 1$ for this reference model. All of the power spectra used in this paper are calculated using the transfer function fitting formulae of Eisenstein & Hu (1998) and assume a scale-invariant primordial spectrum, unless stated otherwise. We have parametrized the model power spectra explicitly by $P(k, \Omega_m h, \Omega_b/\Omega_m)$ in order to avoid confusion with differing definitions of the commonly used shape parameter Γ.

The raw results are gratifyingly accurate, with fractional errors in the power of only ~ 15 per cent out to $k = 0.02\,h\,\mathrm{Mpc}^{-1}$. To within about 20 per cent, the observed spectral shape is that of the $P(k, \Omega_m h = 0.2, \Omega_b/\Omega_m = 0)$ reference model between $0.02\,h\,\mathrm{Mpc}^{-1} < k < 0.6\,h\,\mathrm{Mpc}^{-1}$. At smaller scales, the Finger-of-God redshift-space smearing is clearly seen to reduce the power. In many ways, the most striking features are the suggestions of oscillatory modulations, with a possible peak at $k \simeq 0.065\,h\,\mathrm{Mpc}^{-1}$ and possible troughs at $k \simeq 0.035\,h\,\mathrm{Mpc}^{-1}$ and $k \simeq 0.1\,h\,\mathrm{Mpc}^{-1}$. However, it is clear that the window function has caused adjacent power estimates to be closely correlated, so a proper covariance analysis is required before any significance can be given to these apparent features. Given the precision of the basic power estimates, it is necessary to attain an accurate measure of the systematic effects listed above that modify the shape of the spectrum. We achieve this in the next Section by using mock data.
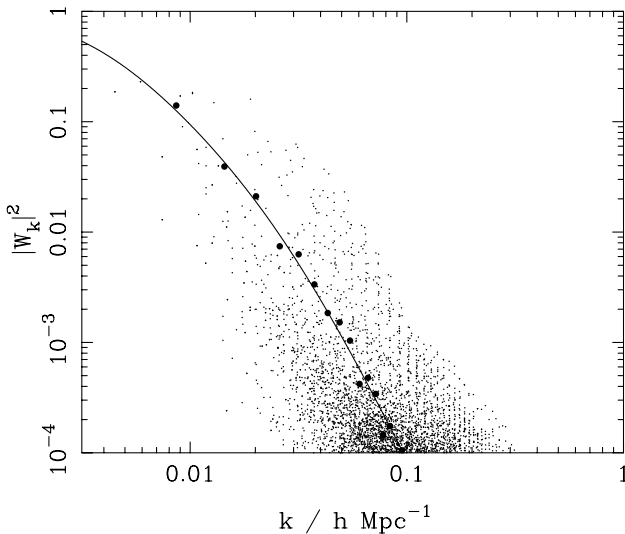

Figure 1. The 2dFGRS window function in Fourier space. The fitting formula of equation (4) is plotted (solid line) compared to the spherically averaged power obtained by Fourier transforming a random catalogue created to match the 2dFGRS window function (solid circles). This catalogue, containing five times as many points as the true galaxy catalogue was placed on a $512 \times 512 \times 256$ grid that encompassed all the data. Values from individual grid points are also plotted (dots), and show the anisotropy of the window function.

4   TESTS ON MOCK DATA

Redshift-space and non-linear effects mean that the shape of the recovered power spectrum gives information about the linear power spectrum only at small values of k. The easiest way to model both these effects is via numerical simulation. Using an empirically motivated biasing scheme, it is possible to place galaxies within N-body simulations and provide mock catalogues designed to mimic the 2dFGRS catalogue for different cosmological models (Cole et al. 1998; Baugh et al., in preparation). In this section we
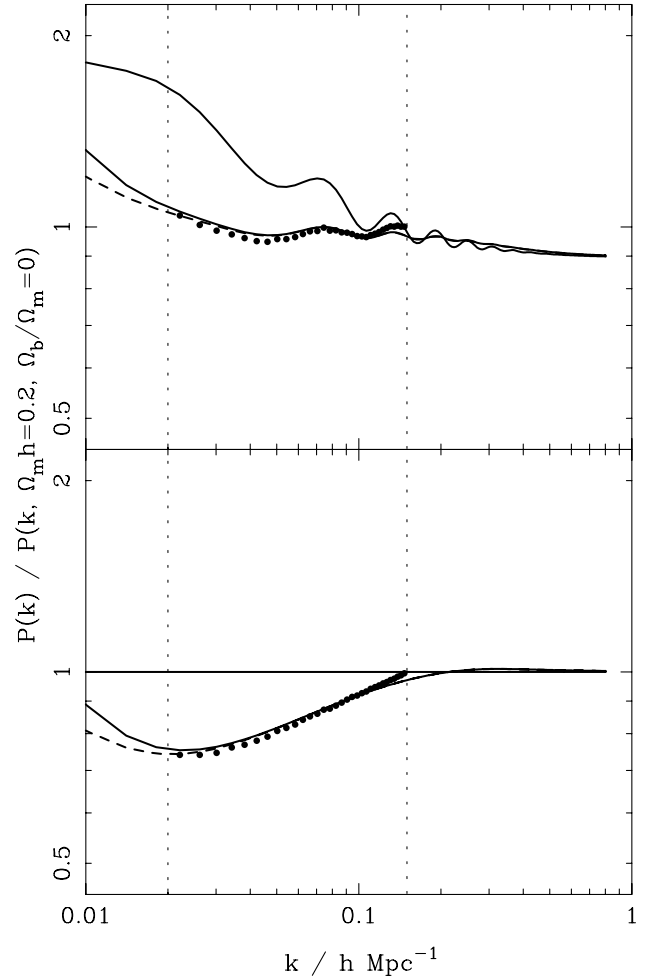

Figure 2. The effect of convolving a linear power spectrum with the 2dFGRS window function. Two model power spectra are compared: the top panel shows a power spectrum including a baryonic component $P(k, \Omega_m h = 0.2, \Omega_b/\Omega_m = 0.16)$, while the bottom panel shows a power spectrum $P(k, \Omega_m h = 0.2, \Omega_b/\Omega_m = 0)$ with no baryonic component. These spectra are divided by a smooth reference model, $P(k, \Omega_m h = 0.2, \Omega_b/\Omega_m = 0)$. The upper solid lines show the unconvolved power spectra, and the lower solid lines show the power spectra convolved with the fit to the window function given by equation (4). The dashed lines show the average power spectrum expected from data which has had the average over-density artificially set to zero (see Section 3.2 for details). Solid symbols show the shape of the average recovered power spectrum from 1000 Gaussian realizations of the density field (with different phases), place on a $256 \times 256 \times 128$ grid at locations covered by the 2dFGRS. Because of the relatively coarse grid used, aliasing swamps the signal at $k > 0.15\,h\,\mathrm{Mpc}^{-1}$, and data are only shown for the range of k over which the 2dFGRS power spectrum is fitted (Section 6). This region is delineated by the vertical dotted lines.

use these mock catalogues to demonstrate that for $k < 0.15\,h\,\text{Mpc}^{-1}$ the only important effect on the power spectrum is the convolution with the window function.

Fig. 4 shows a collection of power spectra calculated from samples drawn from the ΛCDM and τCDM Hubble volume simulations (see Cole et al. 1998; Baugh et al., in preparation, and http://star-www.dur.ac.uk/~cole/mocks/main.html for details). The large catalogues constructed in this work were re-sampled depending on angular position and redshift to match the correct window function for the 2dFGRS data. Power spectra were calculated exactly as for the 2dFGRS data. Fig. 4 illustrates the factors that transform the linear mass power spectrum into the non-linear galaxy spectrum. Panel (a) shows the power spectrum of the mass at $z = 0$. This demonstrates the increase in power on small scales caused by the collapse of haloes. Panel (b) differs in that we now have to consider the effect of bias (artificially added to the simulation), and the window function. In panel (c), we analyse samples designed to mimic the 2dFGRS data as closely as possible, including redshift-space effects: the Finger-of-God effect that decreases small-scale power, and the Kaiser effect that enhances the power. The redshift-space and non-linear effects cancel to some extent and give approximately the correct level of $P(k)$ out to $k \sim 0.5\,h\,\text{Mpc}^{-1}$. However, the shape of the power spectrum is altered for $k \gtrsim 0.2\,h\,\text{Mpc}^{-1}$.

We will therefore assume that, at $k < 0.15\,h\,\text{Mpc}^{-1}$, redshift space distortions and non-linear effects have an insignificant effect on the shape of $P(k)$. Allowing the normalization to vary removes any large-scale constant bias; the bias is not expected theoretically to vary significantly with k on these large scales (Kauffmann, Nusser & Steinmetz 1997; Benson et al. 2000). In the future, measurements of $\beta \equiv \Omega_m^{0.6}/b$ from redshift-space distortions as a function of scale will test directly the degree to which this is true (see Peacock et al. 2001 for the first 2dFGRS results on redshift-space distortions). This region of the power spectrum therefore directly provides information about the shape of the linear power
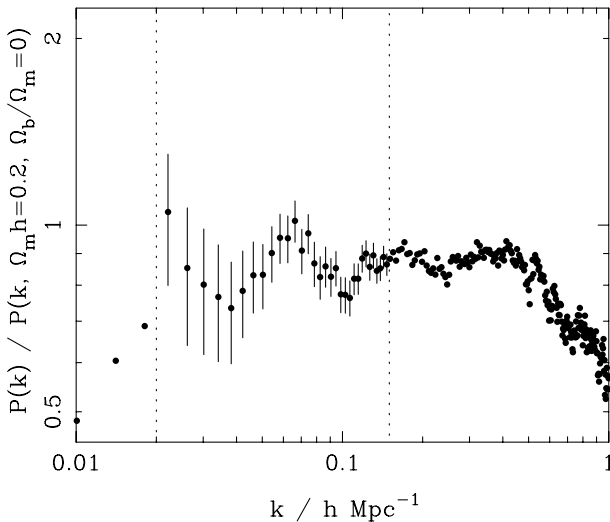
spectrum, and can be used with models of the transfer function to provide constraints on cosmological parameters. Although this conclusion has only been justified here for two specific assumed models, we have performed similar tests on a wider range of models. In Table 1, we show explicitly how the results depend on the range of wavenumber considered.

5   ESTIMATING THE COVARIANCE MATRIX

The $P(k)$ data points in Fig. 3 are not independent, and correlations extend across finite regions of k-space. This is predominantly caused by the convolution with the window function, although there is also a contribution from non-linear effects (Meiksin & White 1999; Scoccimarro, Zaldarriaga & Hui 1999) and redshift-space effects. Particular care must therefore be taken in interpreting 'wiggles' in the power spectrum as significant features. In order to quantify these correlations, we have estimated the covariance matrix for the data points with $k < 0.15\,h\,\text{Mpc}^{-1}$.

A large number of independent realizations of $P(k)$ are required in order to have sufficient signal-to-noise in the covariance matrix. It would be too time-consuming to perform separate numerical simulations for each data set. Instead, we have created 1000 realizations of a Gaussian random field on a $256 \times 256 \times 128$ grid covering the region of the 2dFGRS survey. For $k < 0.15\,h\,\text{Mpc}^{-1}$, using a smaller grid than that used for the 2dFGRS data does not significantly affect the result, and reduces the computational burden. The resulting power spectra, determined as for the 2dFGRS data, were used in Section 3.2 to demonstrate the effect of convolving $P(k)$ by the window function. These realizations provide an estimate of the cosmic variance within the 2dFGRS volume. The contribution from shot noise has been calculated by analysing similar Monte Carlo realizations, and has been included in our estimate of the covariance matrix.

Estimating the covariance matrix in this way does not take into account non-linear and redshift-space effects, which add to the covariances. However, these effects should be small over the region of k-space that we are fitting. As a test of this, we have estimated the covariance matrix using 10 catalogues drawn from $\Omega_m h = 0.25$ $\Omega_b/\Omega_m = 0$ CDM simulations with different phases by Cole et al. (1998). These catalogues were calculated using Cole et al. (1998) bias model 1. The correlations calculated over the k-space region $0.02 < k < 0.15\,h\,\text{Mpc}^{-1}$ were similar in scale to those calculated from the Gaussian fields. However, we find that the errors in $P(k)$ calculated from numerical simulations are 16 per cent larger than those determined from Gaussian simulations, although there is no evidence for a change in shape of the diagonal elements of the covariance matrix for $k < 0.15\,h\,\text{Mpc}^{-1}$. We do see a change at $k > 0.15\,h\,\text{Mpc}^{-1}$ that is consistent with non-linear and redshift-space effects, which are expected to be an increasing function of k. In this work we adopt the conservative approach and renormalize the covariance matrix calculated from the Gaussian realizations to match the normalization of the numerical simulations, whilst keeping the correlation matrix the same. This renormalization does not significantly affect the primary results of this paper: the derived best-fitting parameters are the same with or without this renormalization.

Figure 3. The 2dFGRS estimate of the redshift-space galaxy power spectrum, expressed as the ratio to a linear-theory CDM $P(k, \Omega_m h = 0.2, \Omega_b/\Omega_m = 0)$ power spectrum with $n = 1$ & $\sigma_8 = 1$. These data do not estimate the true power spectrum, but give the power spectrum convolved with the window function (see Section 3.2). Error bars are determined from the diagonal elements of the covariance matrix (calculated in Section 5), for the $0.02 < k < 0.15\,h\,\text{Mpc}^{-1}$ data constrained by the vertical dotted lines. This is the region fitted in Section 6.4.

6   FITTING TO THE POWER SPECTRUM

6.1   Model parameters

Model power spectra for different cosmologies have been created
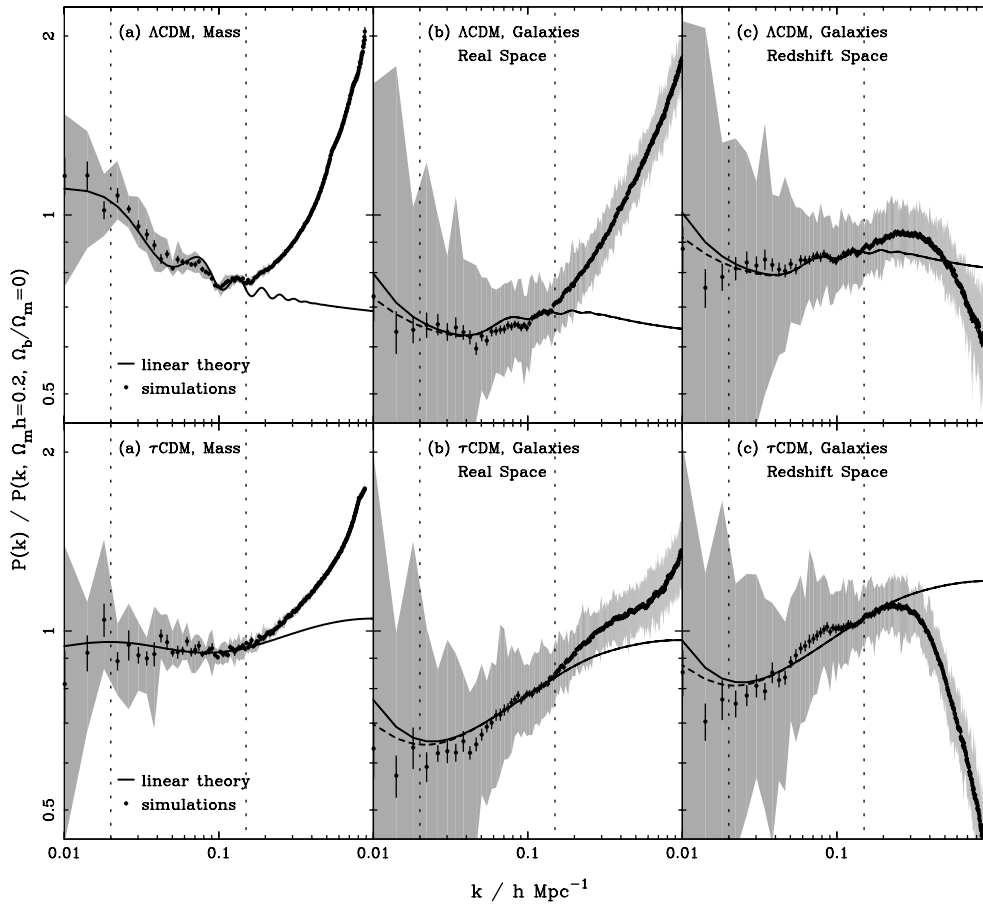
Figure 4. A comparison of power spectra determined from the results of the ΛCDM and τCDM Hubble volume simulations divided by a $P(k, \Omega_m h = 0.2, \Omega_b/\Omega_m = 0)$ reference model. Panel (a): the average spectrum recovered from the $z = 0$ distribution of mass in 8 cubes each of side $1500 \, h \, \mathrm{Mpc}$ (ΛCDM) or $1000 \, h \, \mathrm{Mpc}$ (τCDM) (solid circles with 1σ errors: the extremal data bound the shaded area), compared to the scaled input power spectrum (solid line). Here, the difference between the two is dominated by the non-linear collapse of small-scale structures at $k > 0.15 \, h \, \mathrm{Mpc}^{-1}$. The τCDM mass power spectrum is compared to a reference model with $\sigma_8 = 0.6$ (rather than $\sigma_8 = 1.0$) in order that it has approximately the same normalization as the other data. Panel (b): the average recovered power spectrum from 35 (ΛCDM) and 30 (τCDM) real-space galaxy catalogues sampled from the simulations to match the 2dFGRS window function (solid circles with 1σ errors: the extremal data bound the shaded area). These are compared with the linear spectrum convolved with the analytic approximation to the window function given by equation (4) (solid line). The difference between these two is dominated by both bias (used to create the galaxy catalogue) and non-linear effects. Panel (c): the average recovered power spectrum from 35 (ΛCDM) and 30 (τCDM) redshift-space galaxy catalogues designed to fully mimic the 2dFGRS redshift-space sample (solid circles with 1σ errors: the extremal data bound the shaded area), and the linear spectrum convolved with the window function (solid line). Here, the differences are caused by all of the factors listed in Section 3.1. The dashed lines in panels (b) and (c) show the power spectrum expected from data in which the average over-density is artificially set to zero (see Section 3.2 for details). The $0.02 < k < 0.15 \, h \, \mathrm{Mpc}^{-1}$ region fitted in Section 6.4 is delineated by the vertical dotted lines. In calculating the error in the average power spectra measured from the simulations, we have assumed that the samples are independent. This is not precisely true, and the errors plotted therefore underestimate the true error.

to compare with the 2dFGRS data using the transfer function fitting formulae of Eisenstein & Hu (1998). These formulae are essentially perfect in the regime of interest, and show that the effect of baryons on the power spectrum is not well-approximated by a change in $\Omega_m h$. These differences are important in order to be able to fit the 2dFGRS data with both parameters. The shape of the power spectrum is primarily dependent on $\Omega_m h$, and only weakly dependent on h. We have therefore chosen to fit $\Omega_m h$ rather than Ω_m. Similarly, the strength of baryon oscillations depend primarily on Ω_b/Ω_m. We have therefore calculated model spectra for cosmologies chosen on a $40 \times 40 \times 40$ grid in $(\Omega_m h, \Omega_b/\Omega_m, h)$ space, covering

$$0.1 < \Omega_m h < 0.8,$$

$$0.0 < \Omega_b/\Omega_m < 0.5,$$

$$0.4 < h < 0.9.$$

(5)

These limits act effectively as uniform prior probability densities

for the parameters. A scale-invariant $n = 1$ primordial spectrum was assumed initially, following results from CMB analysis (e.g. Jaffe et al. 2000). We have numerically convolved these power spectra on the scales $0.02 < k < 0.15 \, h \, \mathrm{Mpc}^{-1}$ using the window function fitting formula presented in Section 3.2. The normalization of the model spectra was allowed to vary to account for an unknown large-scale linear bias.

Following analysis of the data using these model spectra, we have also created models on a finer $40 \times 40 \times 40$ grid covering $0.1 < \Omega_m h < 0.3$, $0.0 < \Omega_b/\Omega_m < 0.4$ and $0.4 < h < 0.9$ in order to further constrain the fit in this region of parameter space.

We emphasize that Ω_m is the total matter density parameter, i.e. $\Omega_m = \Omega_{cdm} + \Omega_b$. Our results are not strongly dependent on Ω_v.

6.2 Results

The likelihood of each model has been estimated using a

Table 1. Maximum likelihood (ML) $\Omega_m h$ and Ω_b/Ω_m parameters for fits to the 2dFGRS power spectrum, varying the range of k-space fitted, the power-law index n of the primordial spectrum and the matter density of the flat cosmology assumed to estimate the comoving distance to each galaxy. The maximum likelihood $\Omega_m h$ and Ω_b/Ω_m parameters are also presented for fits to the power spectra calculated from the NGP and SGP data subsets. For these subsets, the $0.02 < k < 0.15$ data were fitted assuming a scale-invariant primordial spectrum and a flat $\Omega_m = 0.3$ cosmology to estimate the comoving distance to each galaxy. All of these fits used covariance matrices calculated from Gaussian realizations of a $\Omega_m h = 0.2$, $\Omega_b/\Omega_m = 0.16$ CDM power spectrum.

$k\,(h\,\mathrm{Mpc}^{-1})$		n	Assumed Ω_m for $r(z)$	ML parameters	
min.	max.			$\Omega_m h$	Ω_b/Ω_m
0.02	0.15	1.0	1.0	0.23 ± 0.03	0.18 ± 0.07
0.02	0.15	1.0	0.4	0.20 ± 0.03	0.16 ± 0.07
0.02	0.15	0.9	0.3	0.22 ± 0.03	0.12 ± 0.07
0.02	0.15	1.1	0.3	0.18 ± 0.03	0.19 ± 0.07
0.015	0.15	1.0	0.3	0.20 ± 0.03	0.14 ± 0.07
0.03	0.15	1.0	0.3	0.20 ± 0.03	0.15 ± 0.07
0.02	0.10	1.0	0.3	0.17 ± 0.04	0.18 ± 0.08
0.02	0.12	1.0	0.3	0.18 ± 0.03	0.17 ± 0.07
0.02	0.15	1.0	0.3	0.20 ± 0.03	0.15 ± 0.07
NGP data subset				0.18 ± 0.05	0.14 ± 0.10
SGP data subset				0.22 ± 0.04	0.13 ± 0.08

Figure 5. Likelihood surfaces for the best-fitting linear power spectrum over the region $0.02 < k < 0.15\,h\,\mathrm{Mpc}^{-1}$. The normalization is a free parameter to account for the unknown large-scale biasing. Contours are plotted at the usual positions for one-parameter confidence of 68 per cent, and two-parameter confidence of 68, 95 and 99 per cent (i.e. $-2\ln(\mathcal{L}/\mathcal{L}_{\max}) = 1, 2.3, 6.0$ and 9.2). We have marginalized over the missing free parameters (h and the power spectrum amplitude) by integrating under the likelihood surface.

covariance matrix calculated from Gaussian realizations of linear density fields, as described in Section 5. The best-fitting power spectrum parameters are only weakly dependent on the model power spectrum that was assumed in calculating the covariance matrix: we have considered a number of input power spectra and find $\chi^2_{\min}$ close to the expected value for all of them. In fact, we used an iterative procedure leading to this choice of covariance matrix. Initially we adopted a $\Omega_m h = 0.25$, $\Omega_b/\Omega_m = 0$ power spectrum, and then adopted the values $\Omega_m h = 0.2$ and $\Omega_b/\Omega_m = 0.16$ which are close to the best-fitting values determined with this covariance matrix.

The likelihood contours in Ω_b/Ω_m versus $\Omega_m h$ for this fit are shown in Fig. 5. At each point in this surface, we have marginalized by integrating the likelihood surface over the two free parameters, h and the power spectrum amplitude. The result is not significantly altered if the modal or maximum likelihood (ML) points in the plane corresponding to power spectrum amplitude and h were chosen instead. The likelihood function is also dependent on the covariance matrix (which should be allowed to vary with cosmology), although the consistency of the results from covariance matrices calculated for different cosmologies shows that this dependence is negligibly small. Thus $\mathcal{L} \propto \exp(-\chi^2/2)$ in practice.

Fig. 5 shows that there is a degeneracy between $\Omega_m h$ and the baryonic fraction Ω_b/Ω_m. However, there are two local maxima in the likelihood, one with $\Omega_m h \simeq 0.2$ and ~ 20 per cent baryons, plus a secondary solution $\Omega_m h \simeq 0.6$ and ~ 40 per cent baryons.

Assuming a uniform prior for h over a factor of 2 is arguably over-cautious, and we have therefore multiplied by a Gaussian prior $h = 0.7 \pm 10$ per cent in Fig. 6. This corresponds to multiplying by the likelihood from external constraints such as the *Hubble Space Telescope* key project (Freedman et al. 2001). The effect is to tighten the contours around the above two models. The low-density model now becomes approximately

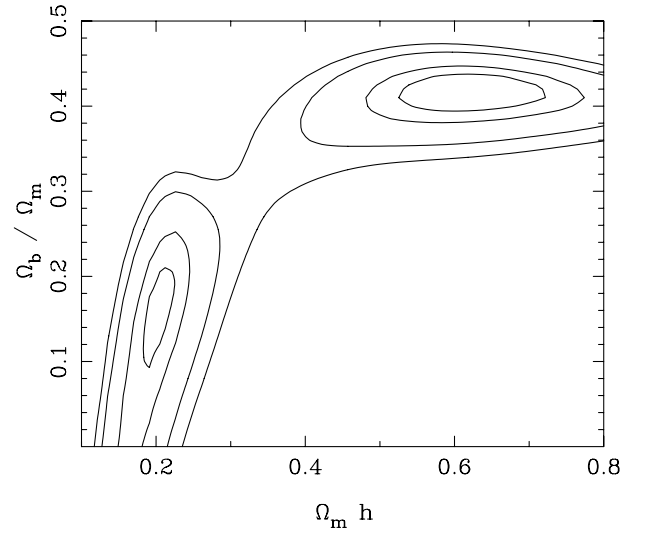$$\Omega_m h = 0.20 \pm 0.03; \qquad \Omega_b/\Omega_m = 0.15 \pm 0.07. \qquad (6)$$

The errors quoted are rms errors, and have been calculated by integrating over the branch of solutions of interest. Analysing mock catalogues drawn from the ΛCDM Hubble volume simulation produces similar rms errors, and shows that, for each parameter, the interval defined by the appropriate error is close to a 68 per cent confidence interval (see Section 6.4).

The 2dFGRS data are compared to the best-fitting linear power spectra convolved with the window function in Fig. 7. This shows where the two branches of solutions come from: the low-density model fits the overall shape of the spectrum with relatively small 'wiggles', while the solution at $\Omega_m h \simeq 0.6$ provides a better fit to the bump at $k \simeq 0.065\,h\,\mathrm{Mpc}^{-1}$, but fits the overall shape less well.

6.3 Robustness of the fit

We have tried varying the range of k for the fit, the assumed power-law index of the primordial fluctuations, and the assumed geometry. The best-fitting $\Omega_m h$ and Ω_b/Ω_m for a variety of assumptions are presented in Table 1 along with approximate errors. $h = 0.7 \pm 10$ per cent was assumed for this analysis. The shape of the likelihood surfaces and the position of the minimum recovered from each of these fits are similar, and the ML values generally change by $\ll 1\sigma$. The main effect of changing assumptions is in how rapidly the likelihood falls away from the ML point.

Perhaps the main point to emphasize here is that the results are not greatly sensitive to the assumed tilt of the primordial spectrum. We have used the CMB results to motivate the choice of $n = 1$, but it is clear that very substantial tilts are required to alter our conclusions significantly: $n \simeq 0.8$ would be required for the zero-baryon model to become an acceptable fit, within 1σ of the preferred model.

We have also fitted models to power spectra calculated from two

subsets of the data, the NGP and SGP excluding random fields. The NGP subset contained 51 862 galaxies, and the SGP subset contained 75 786 galaxies. The redshift-space window functions for these subsets have more simple geometries than the complete sample. Power spectra have been calculated for each subset, as described in Section 3.1. The fit to the spherically averaged
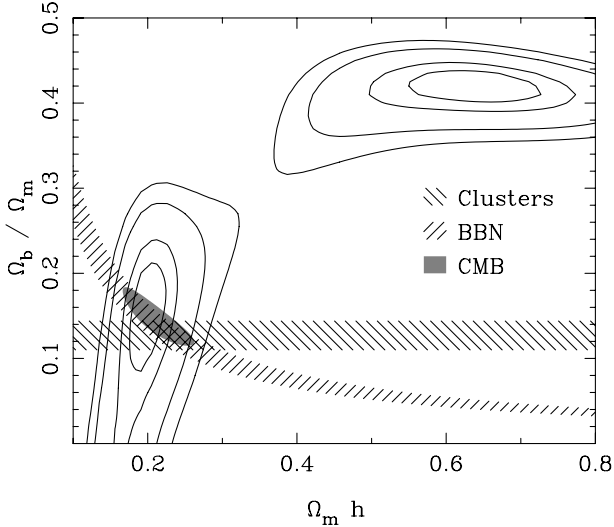

Figure 6. Likelihood surfaces for the best-fitting linear power spectrum over the region $0.02 < k < 0.15\,h\,\mathrm{Mpc}^{-1}$, as in Fig. 5, but now adding a prior on h: $h = 0.7 \pm 10$ per cent. This tightens the constraints. This result is compared to estimates from X-ray cluster analysis (Evrard 1997), big-bang nucleosynthesis (O'Meara et al. 2001) and recent CMB results (Netterfield et al. 2001; Pryke et al. 2001). Note that we have plotted the CMB result following the reasonable approximation that $\Omega_b h^2$ and $\Omega_{cdm} h^2$ were independently determined by each of these analyses.
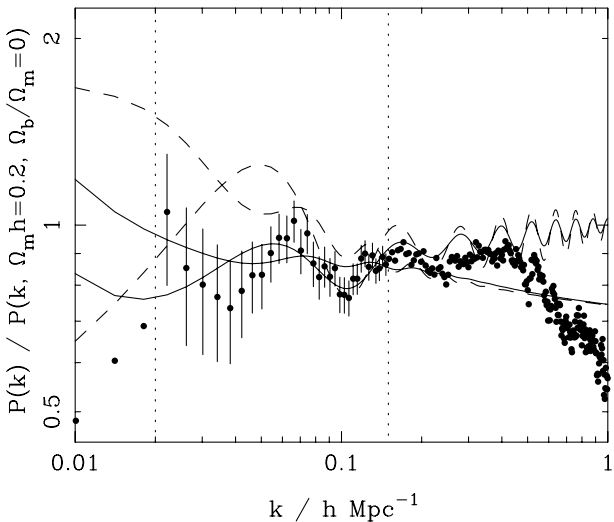

Figure 7. The 2dFGRS data compared with the two preferred models from the maximum likelihood fits convolved with the window function (solid lines). Error bars show the diagonal elements of the covariance matrix, for the fitted data that lie between the dotted vertical lines. The unconvolved models are also shown (dashed lines). The $\Omega_m h \simeq 0.6$, $\Omega_b/\Omega_m = 0.42$, $h = 0.7$ model has the higher bump at $k \simeq 0.05\,h\,\mathrm{Mpc}^{-1}$. The smoother $\Omega_m h \simeq 0.20$, $\Omega_b/\Omega_m = 0.15$, $h = 0.7$ model is a good fit to the data because of the overall shape.

window function and the covariance matrix were also revised for each subset. Results of this analysis are presented in Table 1, and show that the parameters deduced from either subset are consistent with those derived from the complete sample.

6.4 Fitting to mock data

Using the technique described in Section 6.2, we have tried to recover the input parameters of the ΛCDM simulation, $\Omega_m h = 0.21$ and $\Omega_b/\Omega_m = 0.13$, from 35 redshift-space galaxy catalogues drawn from this simulation to mimic the 2dFGRS data. Having calculated power spectra for the catalogues [presented in panel (c) of Fig. 4], we have fitted the data with models using a covariance matrix calculated as in Section 5. The ML (and secondary maxima if present) $\Omega_m h$ and Ω_b/Ω_m parameters recovered from these catalogues are presented in Fig. 8. There is a degeneracy between recovered parameters: the data trace a pattern similar to that of power spectra with similar shape in the region $0.02 < k < 0.15\,h\,\mathrm{Mpc}^{-1}$. This pattern is similar to that determined from the 2dFGRS data (Fig. 6). The degeneracy between $\Omega_m h$ and Ω_b/Ω_m is weakly broken with the models favouring approximately the correct baryon fraction. For each maximum within the region $0.1 < \Omega_m h < 0.3$ and $0.0 < \Omega_b/\Omega_m < 0.4$, we have integrated over the likelihood and find rms values similar to those obtained from the 2dFGRS data. Of the 35 catalogues modelled, 27 (77 per cent) have likelihood maxima within 1 rms of the true $\Omega_m h$ value (i.e. they have likelihood maxima with $0.18 < \Omega_m h < 0.24$). We also find that 24 (69 per cent) have likelihood maxima within 1 rms of the true baryon fraction (i.e. they have likelihood maxima with $0.06 < \Omega_b/\Omega_m < 0.20$). This gives us confidence that the quoted errors for the best-fitting parameters derived from the 2dFGRS data are sound.

Combining the likelihood surfaces calculated from the 13 non-overlapping catalogues results in best-fitting parameters $\Omega_m h = 0.20 \pm 0.15$ and $\Omega_b/\Omega_m = 0.10 \pm 0.05$, with $-2\ln(\mathcal{L}_{true}/\mathcal{L}_{max}) < 1.0$ for the combined likelihood. This offset is statistically acceptable, and suggests that, if there is a systematic bias in determining $\Omega_m h$ and Ω_b/Ω_m from these catalogues, it is at a level well below the errors on the recovered parameters from any single catalogue.

7 CONCLUSIONS

We have shown that the present 2dFGRS data allow the galaxy power spectrum to be measured to high accuracy (10–15 per cent rms) over about a decade in scale at $k < 0.15\,h\,\mathrm{Mpc}^{-1}$. We have carried out a range of tests for systematics in the analysis and a detailed comparison with realistic mock samples. As a result, we are confident that the 2dFGRS result can be interpreted as giving the shape of the linear-theory matter power spectrum on these large scales, and that the statistical errors and covariances between the data points are known.

By fitting our results to the space of CDM models, we have been able to reach a number of interesting conclusions regarding the matter content of the universe:

(i) The power spectrum is close in shape to that of a $\Omega_m h = 0.2$ model, to a tolerance of about 20 per cent.

(ii) Nevertheless, there is sufficient structure in the $P(k)$ data that the degeneracy between Ω_b/Ω_m and $\Omega_m h$ is weakly broken. The
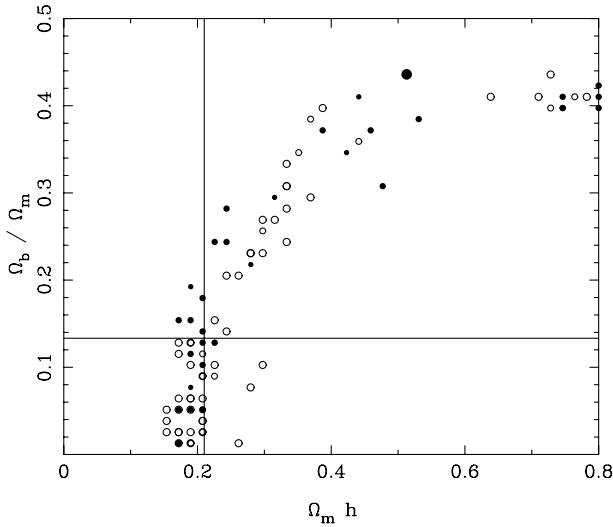
Figure 8. 2D likelihood maxima in the $(\Omega_m h, \Omega_b/\Omega_m)$ plane calculated from 35 redshift-space catalogues drawn from the ΛCDM Hubble volume simulation. We have marginalized (by integrating under the likelihood) over h and $P(k)$ amplitude assuming a Gaussian prior $h = 0.7 \pm 0.07$ and a uniform prior for the amplitude. Primary maxima are given by the solid circles, other maxima with $-2\ln(\mathcal{L}/\mathcal{L}_{max}) < 9.2$ (of which there were ~ 1.7 for each catalogue) by the open circles. Primary maxima for which there was no secondary maximum are shown by the large solid circles. The locus of recovered parameters has a similar pattern to that of power spectra with similar shape over $0.02 < k < 0.15\,h\,\mathrm{Mpc}^{-1}$, and is also similar to that seen in the likelihood contours deduced from the 2dFGRS data. Solid lines mark the input parameters for the simulation.

two local likelihood maxima have $(\Omega_m h, \Omega_b/\Omega_m) \simeq (0.2, 0.15)$ and $(0.6, 0.4)$ respectively.

(iii) The evidence for detection of baryon oscillations in the power spectrum is presently modest, with a likelihood ratio of approximately 2.7 between the favoured model and the best zero-baryon model. Conversely, a large baryon fraction can be very strongly excluded: $\Omega_b/\Omega_m < 0.28$ at 95 per cent confidence, provided $\Omega_m h < 0.4$.

(iv) These conclusions do not depend strongly on the value of h, although they do depend on the tilt of the primordial spectrum, with $n \simeq 0.8$ being required to make a zero-baryon model an acceptable fit to the data.

(v) The sensitivity to tilt emphasizes that the baryon signal comes in good part from the overall shape of the spectrum. Although the eye is struck by a single sharp 'spike' at $k \simeq 0.065\,h\,\mathrm{Mpc}^{-1}$, the correlated nature of the errors in the $P(k)$ estimate means that such features tend not to be significant in isolation. We note that the convolving effects of the window would require a very substantial spike in the true power in order to match our data exactly. Such over-fitting is not possible within the compass of conventional models, and the conservative conclusion is that the apparent spike is probably enhanced by correlated noise. A proper statistical treatment is essential in such cases.

It is interesting to compare these conclusions with other constraints. Averaging the results of Netterfield et al. 2001 and Pryke et al. (2001), the current CMB data require $\Omega_m h^2 = 0.15 \pm 0.03$, $\Omega_b h^2 = 0.0215 \pm 0.0025$, together with a power-spectrum index of $n = 0.97 \pm 0.06$, on the assumption of pure scalar fluctuations. If we take $h = 0.7 \pm 10$ per

cent, this gives

$$\Omega_m h = 0.21 \pm 0.05; \quad \Omega_b/\Omega_m = 0.14 \pm 0.03, \quad (7)$$

in remarkably good agreement with the estimate from the 2dFGRS;

$$\Omega_m h = 0.20 \pm 0.03; \quad \Omega_b/\Omega_m = 0.15 \pm 0.07. \quad (8)$$

Latest estimates of the deuterium-to-hydrogen ratio in quasar spectra combined with big-bang nucleosynthesis theory predict $\Omega_b h^2 = 0.0205 \pm 0.0018$ (O'Meara et al. 2001), in agreement with the latest CMB results. The confidence interval estimated from the 2dFGRS power spectrum overlaps both regions. X-ray cluster analysis predicts a baryon fraction $\Omega_b/\Omega_m = 0.127 \pm 0.017$ (Evrard 1997) which is again within 1σ of our preferred value.

The above limits are all shown on Fig. 6, and paint a picture of impressive consistency: it appears that we live in a universe that has $\Omega_m \simeq 0.3$ with a baryon fraction of approximately 15 per cent. The precision of this statement will improve greatly with completion of the 2dFGRS. Doubling the sample size will improve the errors on the baryon fraction by much more than $\sim\sqrt{2}$. The window function will be more compact, so the signatures of baryon oscillations should be seen very clearly – or we will see that some non-standard alternative is required.

REFERENCES

Baugh C. M., Efstathiou G., 1993, MNRAS, 265, 145
Benson A. J., Cole S., Frenk C. S., Baugh C. M., Lacey C. G., 2000, MNRAS, 311, 793
Cole S., Hatton S., Weinberg D. H., Frenk C. S., 1998, MNRAS, 300, 945
Colless M. M. et al., 2001, MNRAS, in press (astro-ph/0106498)
Efstathiou G., Moody S. J., 2001, MNRAS, 325, 160
Eisenstein D. J., Hu W., 1998, ApJ, 496, 605
Evrard A. E., 1997, MNRAS, 292, 289
Feldman H. A., Kaiser N., Peacock J. A., 1994, ApJ, 426, 23
Freedman W. L. et al., 2001, ApJ, 553, 47
Huchra J. P., Geller M. J., de Lapparant V., Corwin H. G., 1990, ApJS, 72, 433
Jaffe A. et al., 2000, Phys. Rev. Lett., 86, 3475
Kaiser N., 1987, MNRAS, 227, 1
Kauffmann G., Nusser A., Steinmetz M., MNRAS, 286, 795
Lewis I. et al., 2000, MNRAS, submitted
Maddox S. J., Efstathiou G., Sutherland W. J., Loveday J., Peterson B. A., 1990a, MNRAS, 242, 43, P
Maddox S. J., Efstathiou G., Sutherland W. J., Loveday J., 1990b, MNRAS, 243, 692
Maddox S. J., Efstathiou G., Sutherland W. J., 1990c, MNRAS, 246, 433
Maddox S. J., Efstathiou G., Sutherland W. J., 1996, MNRAS, 283, 1227
Meiksin A. A., White M., 1999, MNRAS, 308, 1179
Netterfield C. B. et al., 2001, astro-ph/0104460

O'Meara J. M., Tytler D., Kirkman D., Suzuki N., Prochaska J. X., Lubin D., Wolfe A. M., 2001, ApJ, 552, 718

Peacock J. A. et al., 2001, Nat, 410, 169

Pryke C. et al., 2001, astro-ph/0104490

Saunders W. et al., 2000, MNRAS, 317, 55

Schlegel D. J., Finkbeiner D. P., Davis M., 1998, ApJ, 500, 525

Shectman S. A., Landy S. D., Oemler A., Tucker D. L., Lin H., Kirshner R. P., Schechter P. L., 1996, ApJ, 470, 172

Scoccimarro R., Zaldarriaga M., Hui L., 1999, ApJ, 527, 1

This paper has been typeset from a TEX/LATEX file prepared by the author.